Microchim Acta (2014) 181:1749–1757
DOI 10.1007/s00604-014-1244-3

ORIGINAL PAPER

Resonant gravimetric immunosensing based on capacitive micromachined ultrasound transducers

Darius Virzonis · Gailius Vanagas · Almira Ramanaviciene · Asta Makaraviciute · Dovydas Barauskas · Arunas Ramanavicius · Weijia Wen · Rimantas Kodzius

Received: 1 July 2013 / Accepted: 20 March 2014 / Published online: 8 April 2014

Abstract High-frequency (40 MHz) and low-frequency (7 MHz) capacitive micromachined ultrasound transducers (CMUT) were fabricated and tested for use in gravimetric detection of biomolecules. The low-frequency CMUT sensors have a gold-coated surface, while the high-frequency sensors have a silicon nitride surface. Both surfaces were functionalized with bovine leukemia virus antigen gp51 acting as the antigen. On addition of an a specific antibody labeled with horseradish peroxidase (HRP), the antigen/antibody complex is formed on the surface and quantified by HRP-catalyzed oxidation of tetramethylbenzidine. It has been found that a considerably smaller quantity of immuno complex is formed on the high frequency sensor surface. In parallel, the loading of the surface of the CMUT was determined via resonance frequency and electromechanical resistance readings. Following the formation of the immuno complexes, the resonance frequencies of the low-frequency and high-frequency sensors decrease by up to 420 and 440 kHz, respectively. Finite element analysis reveals that the loading of the (gold-coated) low frequency sensors is several times larger than that on high frequency sensors. The formation of the protein film with pronounced elasticity and stress on the gold surface case is discussed. We also discuss the adoption of this method for the detection of DNA using a hybridization assay following polymerase chain reaction.

Keywords Label-free biomolecule detection · Immunosensing · Capacitive micromachined ultrasound transducers · Gravimetric sensors · Sensor arrays · DNA hybridization

D. Virzonis (✉) · G. Vanagas · D. Barauskas
Department of Technologies, Kaunas University of Technology Panevezys Faculty, Daukanto 12, 35212 Panevezys, Lithuania
e-mail: darius.virzonis@ktu.lt

A. Ramanaviciene · A. Makaraviciute
NanoTechnas – Center of Nanotechnology and Materials Science, Department of Analytical and Environmental Chemistry, Faculty of Chemistry, Vilnius University, Naugarduko 24, 03225 Vilnius, Lithuania

A. Ramanavicius
Department of Physical Chemistry, Faculty of Chemistry, Vilnius University, Naugarduko 24, 03225 Vilnius, Lithuania

A. Ramanavicius
Laboratory of BioNanoTechnology, Department of Material Science and Electrical Engineering, Semiconductor Physics Institute, State Research Institute Center for Physical and Technological Sciences, A. Gostauto 11, 01108 Vilnius, Lithuania

W. Wen · R. Kodzius
KAUST-HKUST Micro/Nanofluidic Joint Laboratory, Kowloon, Hong-Kong

R. Kodzius
Biological and Environmental Science and Engineering Division (BESE), Computer, Electrical and Mathematical Sciences and Engineering Division (CEMSE) and Computational Bioscience Research Center (CBRC), King Abdullah University of Science and Technology, Thuwal 23955-6900, Kingdom of Saudi Arabia

Introduction

Microelectromechanical systems (MEMS) devices, such as micro/nano cantilevers, thin film bulk resonators (FBAR), surface acoustic waves (SAW) devices and capacitive micromachined ultrasound transducers (CMUT) nowadays are commonly being used as resonant, acoustic or gravimetric chemical and biochemical sensors [1–6]. Application of MEMS for label-free chemical/biochemical detection is superior to classical chemical analysis due to their throughput and miniaturization potential. Also MEMS can be comparatively easily integrated with microelectronic circuits. This creates significant potential for distributed, low-power, low-cost chemical and biochemical sensing. Mechanical part of MEMS is to be modified by the molecules that exhibit specific

interaction with the analyte, which preferably binds molecules to the modified surface and thus introduces physical, chemical, and/or biochemical changes. Then corresponding mass and viscosity changes can be detected, such as the change of the resonance frequency, acoustic wave propagation velocity and attenuation [7]. Both micro/nano cantilever [2] and CMUT [1] techniques have been demonstrated to have tens of zeptogram (10^{-21} g) sensitivity. Basic CMUT structure is the array of electrostatically actuated micrometer-sized plates (commonly referred to as "membranes") supported on the isolating posts and having individually sealed vacuum cavities. A sealed CMUT structure is subjected to less damping than a cantilever structure with correspondingly better potential for higher frequencies and higher resonance quality (Q) factor. Thickness-extensional mode resonance used in FBAR devices is even more advantageous over flexural mode resonance (used in cantilevers and CMUTs) since it is considerably less damped during operation in liquids. The drawback of FBARs is the sensitivity, which is still a few orders of magnitude lower. SAW delay-line type structures have similar advantages and disadvantages [5, 7]. In addition to the sensitivity the advantage of the CMUT approach over FBARs and SAW is electrostatic actuation, which eliminates the use of piezoelectric materials and enables the potential to fabricate the devices with standard CMOS technology [8]. CMUTs can also be fabricated in large one-dimensional and two-dimensional arrays of individually wired elements, enabling a number of parallel measurement channels while still maintaining the compact dimensions of an entire device. This results in a high degree of parallelism, which is a great advantage in biosensing, when a high number of different probes is required in a small sensor area. For example, it is recommended to have at least three probe design for the recognition of complimentary DNA strand– the first of which is 100 % complimentary (positive signal), second of which has one or two mismatch (a negative control) and the third one which is not complimentary to the target at all (100 % mismatch). CMUT based biosensing can benefits here from mastered fabrication technologies of compact large arrays, two-dimensional matrixes with bottom side contacts and dedicated electronics [9, 10]. Significant efforts towards matrix sensing have been also made by developers of optical biomolecule sensors, for example by using resonant waveguide gratings with direct 2D imaging and exploiting micropads spatial profiles on a nanopatterned chip [11], however, CMUT platform is still superior in terms of simplicity of readout electronics and ease of integration of sensor with electronic circuits.

We have reported earlier the potential use of CMUTs as immunosensors sensors [6]. In addition to a well known resonance frequency change measurement we have determined significant informative content in the real part of the measured CMUT impedance. However, real-time measurement of the specific interaction of proteins has not been demonstrated yet due to specific requirements for the sensor surface modification, immobilization of proteins and control of the measurement conditions. As specific interaction of biomolecules, such as proteins and DNA takes place in liquid environment, it conflicts with the mass resonance sensor approach, which requires CMUT to be dry in order to maintain the adequate resonance quality. Direct adsorption of antigen on the sensor surface from solution used in our previous work [6], was difficult to control and resulted in comparatively large uncertainty intervals.

In the current work we aim to analyze the relationship between the CMUT surface modification methods and measurement conditions with the changes of CMUT resonance frequency and resistance, which were identified earlier as potentially informative parameters that can give adequate sensing performance.

Experimental

CMUT fabrication and critical data

Two types of CMUTs, having 7 and 40 MHz resonance frequencies were used in this research. Low frequency (7 MHz) devices (LF-CMUT) were fabricated by the wafer bonding process, where 1 μm thick monocrystalline silicon was directly bonded to the 38×38 μm sqare, 150 nm deep cavities fabricated over highly doped and oxidized silicon substrate [12]. Each 0.50×0.25 mm sensor element contains 50 capacitive cells electrically connected in parallel. Three hundred nm thick gold electrodes and bonding pads were deposited and patterned on top of the membranes to provide common conditions for immobilization of biological species as well as to improve electrical coupling to the sensing surface. Figure 1 shows 7 MHz sensor elements (a) and 13-element array wirebonded to the printed circuit board with epoxy passivation of electrical interconnects (c). High frequency (40 MHz) CMUTs (HF-CMUT) were fabricated by the sacrificial release process [13, 14]. 100 nm vacuum gap of 16 μm round capacitive cells was defined by depositing and patterning the sacrificial chromium film over highly doped, oxidized and pre-patterned silicon substrate. 200 nm thick aluminum electrodes were burried between two layers of PECVD silicon nitride films. 140 nm thick bottom and 100 nm thick upper silicon nitride films establish the membrane. Bottom film also plays the role of an isolating layer that prevents CMUT from short circuiting during collapse.

An additional 300 nm layer of PECVD silicon nitride was deposited after sacrificial etching of chromium and critical point drying to seal the etching vias, thus making total plate thickness 740 nm in the electrode area and 540 nm in the rest of the membrane area. Finally bonding pads for top and bottom electrodes were opened. A high frequency sensor contains 2,500 capacitive cells electrically connected in parrallel. Figure 1 shows a 40 MHz sensor element (b) and a

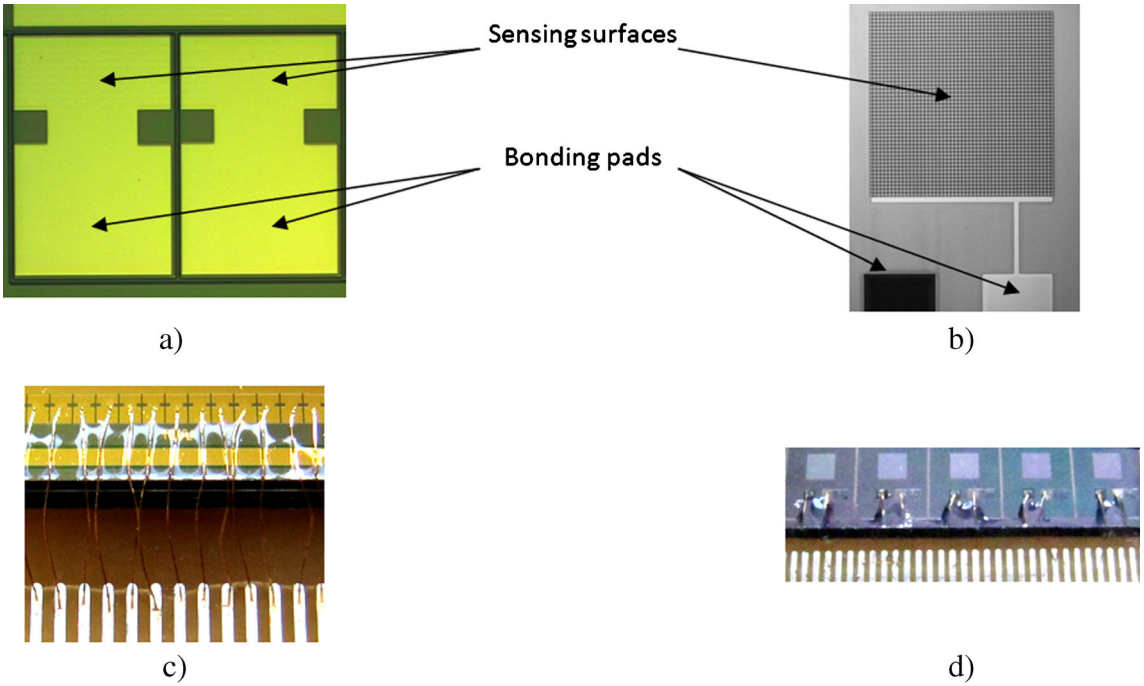

Fig. 1 Micrographs of CMUT sensors: **a** 7 MHz 0.5×0.25 mm multielement sensor with external gold electrodes; **b** 40 MHz 1.3×1.3 mm single sensor with buried aluminum electrode. Photos of mounted and wirebonded sensors: **c** 7 MHz multielement sensor; **d** five 40 MHz sensors in a row

row of five sensors mounted to the printed circuit board with epoxy passivated wirebonding (d). Detailed structure of the capacitive cells is explained in Fig. 2, which also shows the structure of the finite element analysis (FEA) model.

Obtaining sensor readings

Resonance frequency and the values of the real part of the impedance ("resistance") were measured by a network analyzer (Agilent 4395A) equiped with the impedance measurement kit. Forty volt direct current bias was used during all measurements. The resonance frequency and the peak resistance value measured at the resonance were extracted from the measured frequency spectra. Ten elements of LF-CMUT were involved in tests to have more parrallel readings. The HF-CMUT readings were obtained from a single sensor. Measured resonance frequency data initially were interpreted based on the parallel-plate equivalent circuit model described in [14], in relation to the modification of the sensors surface with an increased moving mass of the membrane. For more adequate estimation of non-linear effects induced by the sensor modification and immune complex formation we used the finite element analysis, which is described in the subchapter of this paper.

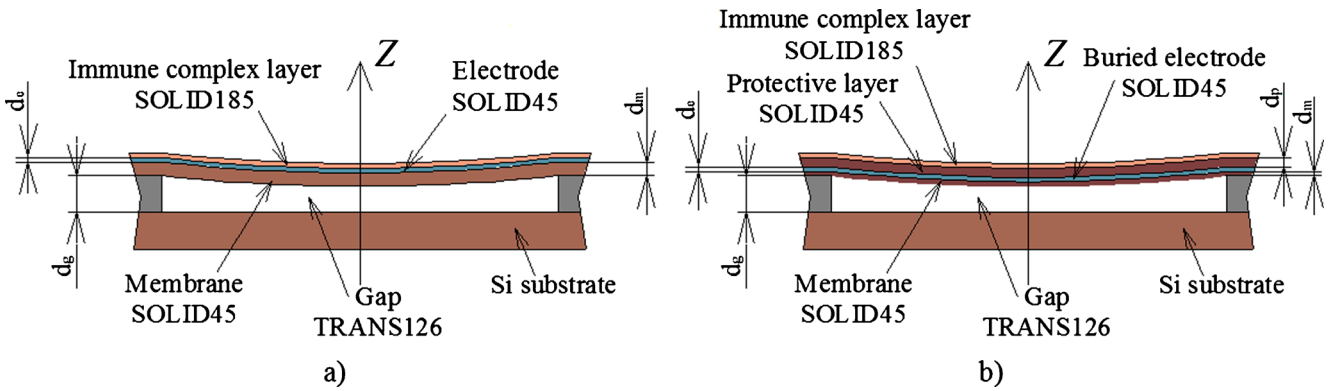

Fig. 2 CMUT capacitive cell structure used in finite element analysis: **a** low frequency sensor cell with surface gold electrode; **b** high frequency sensor cell with burried aluminum electrode

Modification of CMUT with antigen for sensing the interaction with specific anti-gp51-HRP antibody

For the immunoassay and confirmation of the immune complex formation on CMUT we used bovine leukemia virus antigen gp51 (BLV gp51) obtained from BIOK (Kursk, Russia, http://www.biok.ru) and a monoclonal BLV gp51 specific antibody-horseradish peroxidase conjugate (anti-gp51-HRP) from enzootic bovine leukemia virus gp51 antibody test kit (IDEXX Laboratories, Westbrook, Maine, USA, http://www.idexx.com). BLV gp51 (33 μg mL^{-1}) was deposited on the gold coated LF-CMUT surface and on the silicon nitride surface of HF-CMUT. After drying, the deposit was cross-linked covalently by exposing it to glutaraldehyde vapour. Covalent cross-linking of BLV gp51 molecules was performed exploiting the volatility of the glutaraldehyde according to the procedure described earlier [15]. The CMUT surface modified with BLV gp51 was exposed to 25 % glutaraldehyde vapour for 15 min at 20 °C. By using this method covalent bonds were formed between the proteins using bifunctional reagent with aldehyde groups that react with primary amines of amino acid residues. Chemical modification of soluble proteins due to the cross-linking result in minimal changes on the original protein structure [16]. As a result, a thin BLV gp51 layer was formed on the surface allowing further interaction with specific antibodies. The same modification procedure was used for gold and silicon nitride surfaces. Then, the sensor surface modified by BLV antigen gp51 was allowed to react with anti-gp51-HRP for 20 min (concentrated anti-gp51-HRP conjugate was diluted in water at a ratio of 1:100 v.v.). After each deposition, immobilization or interaction step the sensor surface was rinsed with deionized water and dried in the air at the room temperature for 10 min or until no remaining wet residues were observed. Both resonance frequency and electromechanical resistance of the sensors were measured after each step by the network analyzer, so the sensor loading was completely traceable. In order to additionally confirm the formation of immune complexes on the surface (BLV gp51/anti-gp51-HRP), tetramethylbenzydine (TMB) was added as an enzyme substrate. In the presence of an enzyme, the substrate was oxidized resulting in blue colour. The changes of colour were observed in the solution visually, and higher colour intensity was interpreted as a higher complex formation rate. The differences of substrate solution colours collected from all elements with gold and silicon nitride surfaces was very clear and visually easy to distinguish. Thus, in our experiments TMB was used only for qualitative comparison of different surfaces. To evaluate how the readings of the sensors were impacted by complete drying, after the tests, sensors were rinsed and dried as usual and then subjected to 4-day aging in room conditions. After the aging, measurements of the resonance frequency and electromechanical resistance were repeated.

Synthesized oligonucleotides

DNA probes and target representing the sex determining region Y (SRY) gene marker synthesized for hybridization tests are shown in a Table 1 (see also [17]). Positive probes are 100 % complementary to the target DNA, while single mismatch negative probes have a non-complementary base in the middle of the sequence and totally negative probe is non-complementary to the target at all.

Sensor surface regeneration

The surface of CMUT after measurements and tests was brought to the initial state by cleaning the sensing surfaces with oxygen plasma. Cleaning was performed in 3-min steps in reactive ion etching process chamber (Vision 320RIE) at 250 W, 60 mTorr pressure and 80 sccm O_2 flow. Each etching step was followed by the resonance frequency and resistance values measurement to gather the information of gradual unloading of the CMUT structure.

Finite element analysis

To estimate the resonance behavior of CMUT and explain the readings obtained during sensoric CMUT operation we developed the finite element model; its structure is schematically shown in Fig. 2. A single capacitive CMUT cell, which is the basic element of the sensors, was simulated as a complex

Table 1 DNA probes and target representing the SRY gene marker

Oligo name	5′-modification	Sequence	3′-modification	Purpose
Thiol-SRY23pos	disulfide linkage	ATAAGTATCGA**C**CTCGTCGGAAG	None	Positive probe
Thiol-SRY23neg	disulfide linkage	ATAAGTATCGA**A**CTCGTCGGAAG	None	Single mismatch negative probe
SRY24-ThiolPos	None	GCGAAGATGCT**G**CCGAAGAATTGC	disulfide linkage	Positive probe
SRY24-ThiolNeg	None	GCGAAGATGCT**A**CCGAAGAATTGC	disulfide linkage	Single mismatch negative probe
Thiol-NonComp100neg	disulfide linkage	CGAGTCCGCGT**G**CCTACTATTACT	None	Total negative probe
3-47SRY	None	GCAATTCTTCGGCAGCATCTTC GCCTTCCGACGAGGTCGATACTTAT	None	Target DNA

structure: layered membrane supported over the vacuum cavity with isolating posts. Finite element analysis package ANSYS (Canonsburg, PA) was used for simulation. Two membrane types, corresponding to two kinds of CMUT sensors used in this work, were simulated. LF-CMUT (Fig. 2a): square, 1 μm thick monocrystalline silicon membrane with 38 μm side dimension and 300 nm thick gold electrode on top. HF-CMUT (Fig. 2b): 16 μm diameter disc shaped membrane composed of three layers – 140 nm thick silicon nitride isolation layer, 200 nm thick aluminum electrode and 400 nm thick upper membrane layer. In both cases membranes were perimeter-fixed. Each CMUT structure layer was divided by 3D SOLID45 elements, but the very top layer, representing protein film, was divided by 3D SOLID185 elements. This layer mimicked the layer of proteins established after surface modification and immune complex formation. For increased adequacy of the model we made several assumptions, explained in the corresponding paragraph. The vacuum gap was divided by TRANS126 elements. Bias voltage and ambient pressure were preset as initial boundary conditions.

Simulated electromechanical impedance of a CMUT cell was calculated using harmonic analysis results obtained as an output of the model. Generic equation for complex impedance calculation was used [18]:

$$Z_m = \frac{\mathrm{Im}\Delta d_{eff}}{\omega\varepsilon_0\varepsilon_g A_m} + j\frac{d_g - \mathrm{Re}\Delta d_{eff}}{\omega\varepsilon_0\varepsilon_g A_m} + j\frac{d_m}{\omega\varepsilon_0\varepsilon_m A_m} + j\frac{d_i}{\omega\varepsilon_0\varepsilon_i A_m} \quad (1)$$

Here $\omega=2\pi f$ is cyclic frequency; f stands for the oscillation frequency; Δd_{eff} is effective deflection of the membrane; d_g stands for the nominal height of the vacuum gap; d_m is the thickness of the membrane; d_i stands for the isolation layer thickness; A_m is an area of the membrane, which in our case is equal to the electrode area; ε_0, ε_g, ε_m and ε_i are vacuum dielectric constant and dielectric permitivities of the gap, membrane and isolation layer respectively. Calculated sole-cell impedance spectra were extrapolated to the entire senor area dividing calculated values by the number of the cells in the sensor.

Several assumptions regarding the morphological and mechanical properties of the established layer based on biomolecules were made. First, analyzed molecules were thought to inherit elasticity and mass density properties of bovine serum albumine, which are 13.2 GPa and 1,170 kg·m^{-3} correspondingly, according to [19]. Second, when analyzing the initial modification step of LF-CMUT based on BLV gp51 adsorption on the gold surface followed by cross-linking with glutaraldehyde, it was thought that porous layer based on randomly oriented/distributed biomolecules structure having thickness from 300 to 500 nm, which is equivalent to several tens of molecules, was established. Such assumption explains the increase of resonant frequency observed by the LF-CMUT after the initial modification step. The morphology of biomolecule-based layer was supposed to be uniform in the case of HF-CMUT. The difference in behaviours of LF-CMUT and HF-CMUT was caused by different coverage of resonators of these CMUTs, because the adsorption of BLV gp51 protein based layer on gold-coated surface was much higher. Such assumption explains the increase of resonant frequency observed by the LF-CMUT after the initial modification step (this was not the case in HF-CMUT).

The porosity of the protein layer was estimated during FEA by substituting the original elasticity modulus and mass density values with the values characteristic of porous material. The porosity factor, describing the ratio between the mass density of the porous material to the mass density of the bulk material [20] was taken 0.7, which resulted in effective elasticity modulus of 6.5 GPa and mass density of 819 kg·m^{-3}. This filling factor was increased to 1.0 to reflect the mass increase due to the immune complex formation.

We also assumed that in the case of LF-CMUT formed BLV gp51 layer has developed additional intrinsic stress after drying, which was in the range of 10 MPa. This assumption proved to match the experimental data. To distinguish between the newly formed and fully dried (4-day aging) immune complex we simulated an extra 100 nm layer with 1,000 kg·m^{-3} mass density (equivalent to water) for the newly formed immune complex.

Results and discussion

Testing of fabricated CMUTs

After fabrication the sensors underwent functionality tests, common for CMUT. One of the tests, namely frequency spectra evolution of the HF-CMUT in respect of the bias voltage, is presented in Fig. 3. The shift of the resonance frequency and increase of the peak resistance is related to the decreasing gap; the increasing efficiency is due to the increasing bias voltage [12, 14].

Immunoassay sensing tests of LF-CMUT

Low frequency 10 channel multisensor surface modification with glutaraldehyde crosslinking of BLV gp51 and subsequent interaction with anti-gp51-HRP gave CMUT resonance frequency and peak resistance readings shown in Fig. 4a. For better representation we excluded from the diagram the readings of four sensor elements, which exhibited very little or no shift of the resonance frequency and/or resistance. Readings were normalized to the natural resonance frequency values of unmodified sensor to eliminate the scatter of initial parameters. The term “natural resonance frequency” used here can also be understood as a background signal of unmodified sensor. One can observe the increase of resonance frequency and corresponding decrease of the peak resistance after the

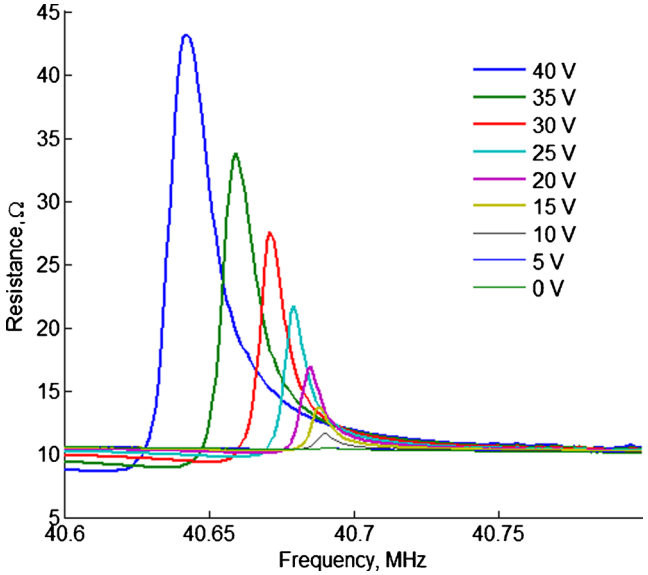

Fig. 3 Evolution of the spectra of the high frequency (40 MHz) sensor in respect the bias voltage

surface modification step. This conflicts with the linear model stating that extra mass deposited on the CMUT surface decreases the resonance frequency [14]. We attribute this to the possibility that the modified surface after crosslinking, rinsing and drying develops extra stress and stiffness, which increases overall spring constant of CMUT membrane and competes with the effect of the increased moving mass. We simulated this behaviour by finite element analysis as described in the Experimental section. The effect of simulated sensor surface modification and immune complex formation on the impedance frequency spectra is shown in Fig. 4b). These spectra were obtained by adding 300 nm thick layer with 13 GPa Young modulus, 1,170 kg·m^{-3} mass density and 0.7 fill factor (see explanation in Experimental section) over the CMUT structure to simulate the initial surface modification step. The filling factor was increased to 1.0 to reflect the immune complex formation. In Fig. 4a) FEA output illustrates each sensing step by dashed and dotted lines. The line ends show the limits of simulated sensor readings corresponding to different protein layer thickness, from 300 to 500 nm. Also the average mass of the protein layer corresponding to the single CMUT cell, as derived from the model output, is indicated. For the best match to the experimental results we also adjusted intrinsic stress and mechanical loss factor in the protein layer for each simulated case. After interaction with anti-gp51-HRP resonance frequency decreased by 3 % (204 kHz) on average; maximum decrease is 6 % (420 kHz). The resistance increased by 38 % (4.2 Ω) on average with maximum increase by 51 % (5.8 Ω). The dark-blue colour of the solution after TMB wetting of the CMUT surface and after the measurement confirmed the immune complex formation.

The results of this experiment confirm the informativity of the sensor and adequacy of the surface modification technique. Sensor readings were repeatedly measured after 4-day aging.

Repeated measurements showed only partial degradation of the sensor readings, namely 17 % decrease of the resistance if compared to the readings of as-formed complex and less than 1 % increase of the resonance frequency.

Immunoassay sensing tests of HF-CMUT

Surface modification and test measurements of the HF-CMUT was performed simultaneously with previously described LF-CMUT tests and the same previously described method with only one difference was used: the high frequency sensor provided silicon nitride surface instead of gold. Sensor readings are presented in Fig. 5a) in the form of the spectra obtained by the network analyzer. Here we observe continuous decrease of the resonance frequency and increase of the resistance due to the surface modification and immune complex formation. After surface modification by BLV gp51 the resonance frequency decreases by 210 kHz (0.5 %) and the resistance increases by 0.5 Ω (6.2 %). As expected, this is the effect of increased mass on CMUT surface without significant build-up of extra stress and elasticity.

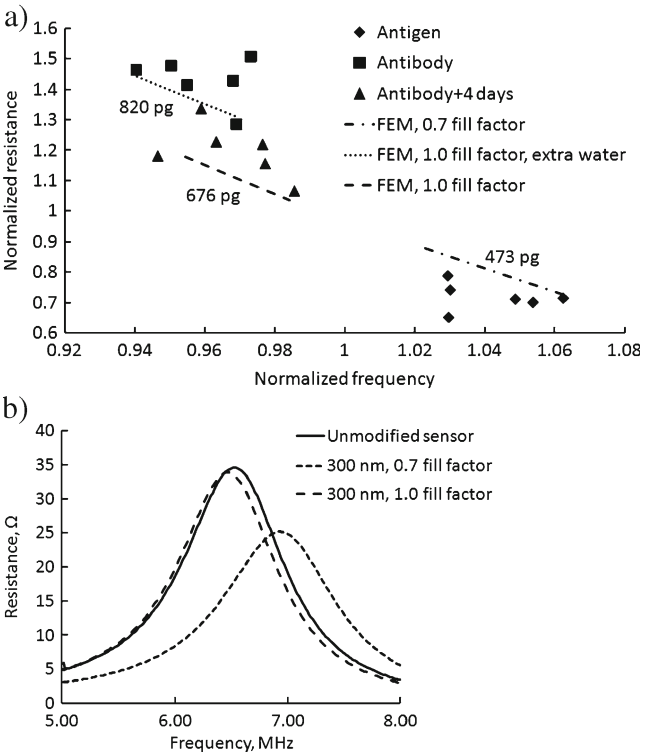

Fig. 4 Low frequency multisensor readings: **a** obtained from 6 elements after surface modification with antigen (BLV gp51) and after interaction with antibody (anti-gp51-HRP); **b** simulated sensor spectra

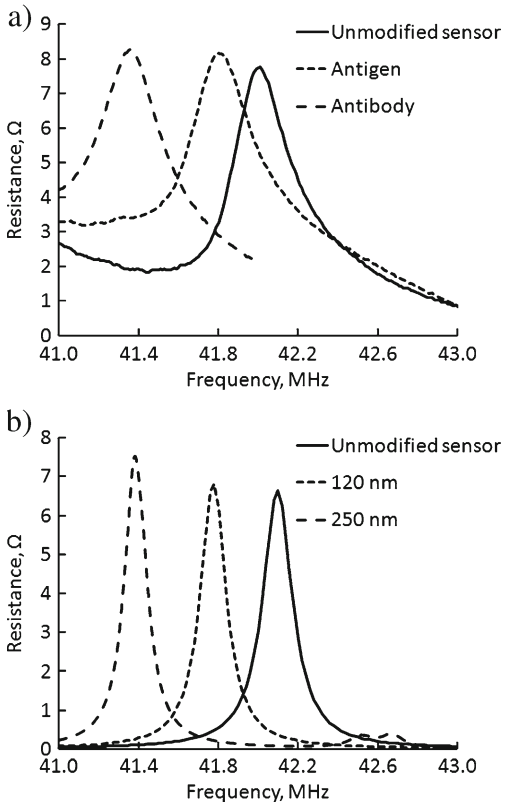

Fig. 5 High frequency (40 MHz) sensor readings (**a**) and simulated readings (**b**)

After interaction with the analyte (anti-gp51-HRP) the tendency of further decrease of the resonance frequency and significant increase of the resistance prevails: frequency is further decreased by 440 kHz (1.1 %) and resistance is increased by 0.2 Ω (2.5 %).

The intensity of the blue colour of TMB deposited on the HF-CMUT surface after the immune complex formation was lower than in the LF-CMUT case, confirming lower density of immobilized antigens and correspondingly a lower ammount of complexes formed.

Figure 5b) shows the evolution of the HF-CMUT impedance frequency spectra simulated by finite element analysis. We used the same simulation technique as for the LF-CMUT, except the representation of the protein layer. Surface modification was simulated by adding a continuous 120 nm thick layer with 1,170 $kg \cdot m^{-3}$ mass density and 3.1 MPa elasticity modulus; the immune complex formation was simulated by adding extra 130 nm of the same layer. Thickness of the simulated layer was chosen to provide the best match to the measured resonance frequency changes. For improved match to the measured impedance spectra we also adjusted the coefficient of mechanical losses in the simulated layer. Remaining mismatch of simulated and measured spectra can be attributed to the non-informative parameters of the interconnects and measurement hardware.

CMUT sensor capability to detect hybridization of immobilized molecules

Oligonucleotides are commercially available, with their primary application as primers for PCR. The oligonucleotides can function in a wide range of modifications, such as amine, biotin, thiol functional groups or fluorophore. While silanization of glass permits to attach thiol-bearing DNA, a direct attachment of disulfide-bearing DNA molecules to CMUT surface allows an easy and simple way to functionalize the sensor. A simple assay can be set up to prove CMUT microfluidic systems capability to detect and measure the presence of target specific DNA molecules in the solution. Positive and negative oligonucleotide probes with disulfide linkage group can be used for CMUT surface functionalization: Thiol-SRY23pos, Thiol-SRY23neg, SRY24-ThiolPos, SRY24-ThiolNeg and Thiol-NonComp100neg. The functionalized positive probes will be able to recognize the amplified PCR product [17], or as for simulation purposes, the single stranded DNA oligonucleotide 3-47SRY, while the target single stranded DNA molecule 3-47SRY will not hybridize to the negative probes and will be washed away (Table 1). Therefore sensor will measure the positive signal only for the positive probes. The DNA sensor can be regenerated, as hybridized target molecules can be removed by lowering the pH or by increasing temperature, reconstituting the single stranded probe molecules on the gold surface. As demonstrated previously [21] the DNA target concentrations as low as 4.16 μM could be detected by quarz crystal microbalance working at 50 MHz, and this value probably can be better for CMUT sensors due to much higher sensitivity potential [1, 6].

Sensor surface regeneration

Oxygen plasma cleaning was carried out to test if sensor readings could be brought to the initial state and to have the readings during gradual sensor surface unloading as additional

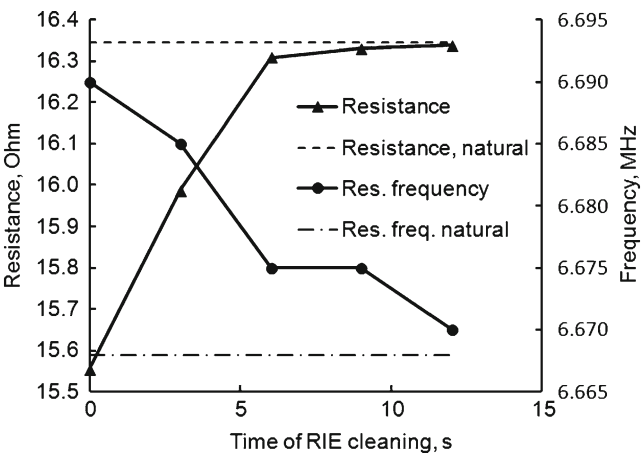

Fig. 6 Sensor unloading by the oxygen plasma reactive ion etching process

reference. Between the oxygen plasma processing steps (3 min each), sensor resonance frequency and resistance were measured. Obtained readings show that sensor resonance frequency and resistance reached initial value, saturating after 6–12 min. The cleaning process is illustrated with one of the low frequency multisensor elements in Fig. 6.

Conclusions

High and low frequency CMUT were fabricated and used for monitoring the specific antigen-antibody interaction. LF-CMUT measurements of BLV gp51/anti-BLV gp51-HRP complex formation have shown that the used concentration of antigen BLV gp51 (33 $\mu g\,mL^{-1}$) layer coated on gold surface after glutaraldehyde cross-linking, rinsing and drying is likely to develop the elasticity value of 13.2 GPa, which causes the LF-CMUT resonance frequency increase by several hundreds of kHz. The influence of protein layer elasticity was not observed in the HF-CMUT case, because, as identified in simulation, the equivalent thickness of protein layer was over two times thinner. We explain it as a result of weak adsorption of BLV gp51 to the silicon nitride surface. The higher BLV gp51 immobilization rate on the gold surface was qualitatively confirmed by the TMB oxidation intensity observed after immune complex formation with anti-gp51-HRP as higher intensity of the blue colour. According to the model parameters fitted to the experimental results we estimate the sensitivity of the LF-CMUT to be not worse than 4.0 fg $(Hz\ cell)^{-1}$ and HF-CMUT not worse than 205 ag $(Hz\ cell)^{-1}$. Better protein adsorption to the gold surface in LF-CMUT case provides the opportunity to lower the concentration of BLV gp51 during initial sensor modification. At the same time, HF-CMUT has better mass sensitivity; this property can be successfully used for sensing low analyte concentrations. We demonstrate that both LF-CMUT and HF-CMUT types of biosensor can be used at room temperature, perform measurements in the solution, are highly sensitive, selective, reproducible and stable. The promising applications of the sensor are determined by biomolecules, such as proteins and DNA in solution.

Acknowledgement This research is funded by a grant (No. MIP-059/2012) from the Research Council of Lithuania.

References

1. Lee HJ, Park KK, Kupnik M, Khuri-Yakub BT (2012) Functionalization layers for CO2 sensing using capacitive micromachined ultrasonic transducers. Sensors Actuators B Chem 174:87–93
2. Long Z, Kou L, Sepaniak MJ, Hou XD (2013) Recent advances in gas phase microcantilever-based sensing. Rev Anal Chem 32(2): 135–158. doi:10.1515/revac-2012-0034
3. Johnston ML, Kymissis I, Shepard KL (2010) FBAR-CMOS oscillator array for mass-sensing applications. Ieee Sens J 10(6):1042–1047. doi:10.1109/Jsen.2010.2042711
4. Tigli O, Bivona L, Berg P, Zaghloul ME (2010) Fabrication and characterization of a surface-acoustic-wave biosensor in CMOS technology for cancer biomarker detection. Ieee Trans Biomed Circ Syst 4(1):62–73. doi:10.1109/Tbcas.2009.2033662
5. Senveli SU, Tigli O (2013) Biosensors in the small scale: methods and technology trends. Iet Nanobiotechnol 7(1):7–21. doi:10.1049/iet-nbt.2012.0005
6. Ramanaviciene A, Virzonis D, Vanagas G, Ramanavicius A (2010) Capacitive micromachined ultrasound transducer (cMUT) for immunosensor design. Analyst 135(7):1531–1534. doi:10.1039/C0an00104j
7. Voiculescu I, Nordin AN (2012) Acoustic wave based MEMS devices for biosensing applications. Biosens Bioelectron 33(1):1–9. doi:10.1016/j.bios.2011.12.041
8. Lemmerhirt DF, Cheng XY, White RD, Rich CA, Zhang M, Fowlkes JB, Kripfgans OD (2012) A 32 x 32 capacitive micromachined ultrasonic transducer array manufactured in standard CMOS. Ieee Trans Ultrason Ferr 59(7):1521–1536. doi:10.1109/Tuffc.2012.2352
9. Zhang XF, Wygant IO, Lin DS, Kupnik M, Oralkan O, Khuri-Yakub BT (2009) Wafer-bonded 2-D CMUT arrays incorporating through-wafer trench-isolated interconnects with a supporting frame. Ieee Trans Ultrason Ferr 56(1):182–192. doi:10.1109/Tuffc.2009.1018
10. Vanagas G, Virzonis D, Paukstaitis V, Baranauskas D, Cerviakov S (2010) Integrated front end electronics design for micromachined ultrasound transducers. Elektron Elektrotech 7:117–120. doi:10.5755/J01.Eee.18.9.2804
11. Bougot-Robin K, Kodzius R, Yue W, Chen L, Li S, Zhang XX, Benisty H, Wen W (2013) Real time hybridization studies by resonant waveguide gratings using nanopattern imaging for Single Nucleotide Polymorphism detection. Biomed Microdevices. doi:10.1007/s10544-013-9832-2
12. Vanagas G, Virzonis D, Mikolajunas M (2008) Testing the capacitive micromachined transducers produced with wafer bonding process. Itelm'2008: Intelligent Technologies in Logistics and Mechatronics Systems:132–139
13. Morkvenaite-Vilkonciene I, Virzonis D, Vanagas G, Krikscikas V (2012) Operating point of capacitive micromachined ultrasonic transducers with sub-structural elements. Elektron Elektrotech 9:43–46. doi:10.5755/J01.Eee.18.9.2804
14. Viržonis D, Vanagas G, Kodzius R (2013) Integration of capacitive micromachined ultrasound transducers to microfluidic devices. In: Panzarella S, Maroni W (eds) Microfluidics: control, manipulation and behavioral applications. Nova, New York City
15. German N, Ramanavicius A, Voronovic J, Oztekin Y, Ramanaviciene A (2011) The effect of gold nanoparticle colloidal solution on performance of glucose oxidase modified carbon electrode. Microchim Acta 172(1–2):185–191
16. Barbani N, Giusti P, Lazzeri L, Polacco G, Pizzirani G (1995) Bioartificial materials based on collagen. 1. Collagen cross-linking with gaseous glutaraldehyde. J Biomater Sci-Polym E 7(6):461–469
17. Wu JB, Kodzius R, Xiao K, Qin JH, Wen WJ (2012) Fast detection of genetic information by an optimized PCR in an interchangeable chip. Biomed Microdevices 14(1):179–186. doi:10.1007/s10544-011-9595-6
18. Ballandras S, Wilm M, Daniau W, Reinhardt A, Laude V, Armati R (2005) Periodic finite element/boundary element modeling of

capacitive micromachined ultrasonic transducers. J Appl Phys 97(3). doi:10.1063/1.1839634

19. Perticaroli S, Nickels JD, Ehlers G, O'Neill H, Zhang Q, Sokolov AP (2013) Secondary structure and rigidity in model proteins. Soft Matter 9(40):9548–9556. doi:10.1039/C3sm50807b
20. Lee D, Wei X, Chen X, Zhao M, Jun SC, Hone J, Herbert EG, Oliver WC, Kysar JW (2007) Microfabrication and mechanical properties of nanoporous gold at the nanoscale. Scri Mater 56(5):437–440. doi:10.1016/j.scriptamat.2006.08.069
21. Bustabad EA, Garcia G, Rodriguez-Pardo L, Farina J, Perrot H, Gabrielli C, Bucur B, Lazerges M, Rose D, Compere C, Arnau A (2009) A biosensor for detection of DNA sequences based on a 50MHz QCM electronic oscillator circuit. 2009 Ieee Sensors 1–3: 687–690. doi:10.1109/Icsens.2009.5398346